

Estimating galaxy masses from kinematics of globular cluster systems: a new method based on deep learning

Rajvir Kaur^{1*}, Kenji Bekki², Ghulam Mubashar Hassan¹ and Amitava Datta¹

¹ *Department of Computer Science and Software Engineering, The University of Western Australia, Australia*

² *International Centre for Radio Astronomy Research (ICRAR), The University of Western Australia, Australia*

4 February 2021

ABSTRACT

We present a new method by which the total masses of galaxies including dark matter can be estimated from the kinematics of their globular cluster systems (GCSs). In the proposed method, we apply the convolutional neural networks (CNNs) to the two-dimensional (2D) maps of line-of-sight-velocities (V) and velocity dispersions (σ) of GCSs predicted from numerical simulations of disk and elliptical galaxies. In this method, we first train the CNN using either only a larger number ($\sim 200,000$) of the synthesized 2D maps of σ (“one-channel”) or those of both σ and V (“two-channel”). Then we use the CNN to predict the total masses of galaxies (i.e., test the CNN) for the totally unknown dataset that is not used in training the CNN. The principal results show that overall accuracy for one-channel and two-channel data is 97.6% and 97.8% respectively, which suggests that the new method is promising. The mean absolute errors (MAEs) for one-channel and two-channel data are 0.288 and 0.275 respectively, and the value of root mean square errors (RMSEs) are 0.539 and 0.51 for one-channel and two-channel respectively. These smaller MAEs and RMSEs for two-channel data (i.e., better performance) suggest that the new method can properly consider the global rotation of GCSs in the mass estimation. We stress that the prediction accuracy in the new mass estimation method not only depends on the architectures of CNNs but also can be affected by the introduction of noise in the synthesized images.

Key words: galaxies:evolution – infrared:galaxies – stars:formation

1 INTRODUCTION

Globular clusters systems (GCSs) of galaxies have long been considered to have fossil information not only on the physical properties of their host galaxies but also on the their hosts’ formation histories e.g., Brodie & Strader (2006), Forbes et al. (2018). Therefore, the physical properties of GCSs such as the projected radial number distributions, kinematics, metallicity distribution functions, and numbers of globular clusters (GCs) per unit galaxy luminosity (“specific frequency”) have been investigated by both observational and theoretical astronomers in various contexts of galaxy formation. For example, the radial density profiles of GCSs have been discussed in the context of suppression of star formation (thus GC formation) in dwarf galaxies by cosmic reionization effects, e.g., Santos et al. (2003), Bekki et al. (2008), Spitler et al. (2012), Griffen et al. (2013), Boylan-Kolchin (2018).

One of the great advantages in studying GCSs in the context of galactic properties is that their kinematics can be used to estimate the total masses of galaxies including dark matter halos well beyond the sizes of their stellar distributions, e.g., Romanowsky et al. (2003) Peng et al. (2004) Alabi et al. (2016). Accordingly, the previous mass estimation of galaxies well beyond their five effective radii (R_e) have provided strong constraints on the total masses of dark matter and their mass fractions, both of which can be compared with corresponding theoretical predictions, e.g., Alabi et al. (2017). Recently, the mass estimation of dark matter in ultra-diffuse galaxies (UDGs) using the kinematics of GCSs made a significant contribution to the better understanding of the UDG formation in clusters of galaxies (e.g., Beasley et al. 2016). The mass estimation of galaxies using GCS kinematics is considered to be complementary to other mass estimation methods using different mass tracers such as planetary nebulae (PNe), e.g., Peng et al. (2004) Morganti et al. (2013) and X-ray gas, e.g., Su et al. (2014).

* corresponding email: 22397217@student.uwa.edu.au

There are a number of ways to estimate the total masses

of galaxies using the radial number density profiles and kinematics of mass tracers like GCs and PNe in galaxies (e.g., Alabi et al. 2016). For example, Romanowsky et al. (2003) used the observed line-of-sight-velocities (V) of 109 PNe in NGC 3379 to estimate the total mass and the mass-to-light-ratio using the spherical Jeans equation with a range of the anisotropy parameter. Peng et al. (2004) used the radial profiles of GC number density, velocity dispersion, and rotation amplitude in NGC 5128 in order to derive the total mass based on the Jeans equation. More recently, Alabi et al. (2016) have applied the new robust mass estimator proposed by Watkins et al (2010) to the observed kinematics of GCSs in 23 early-type galaxies from SLUGGS survey Brodie et al. (2014) in order to derive the total masses of galaxies and the mass fractions of dark matter up to $\sim 13R_e$.

Deep learning has been recently used for various purposes of astronomical studies, such as morphological classification of galaxies, e.g., Dieleman et al. (2015) and determination of mass-ratios of galaxy merging leading to S0 formation, e.g., Diaz et al. (2019). These new methods based on deep learning can dramatically speed up astronomical tasks (e.g., automated galaxy classification without using the human eye) and thus improve the productivity in astronomical research. One of key elements in these studies based on deep learning is to use a large “training dataset”: images of galaxies with different Hubble type for a galaxy classification problem. It is thus possible that deep learning can be applied to the mass estimation of galaxies using kinematics of GCs, if a large number of two-dimensional (2D) maps of GCS kinematics are available for the training dataset.

A possible advantage of the mass estimation method based on deep learning is that the details of 2D kinematics of GCSs can be all used to derive the total masses of galaxies: radial and azimuthal variations of line-of-sight-velocities (V , which can measure global rotation) and velocity dispersions (σ , which can measure random kinetic energy) can be used for the mass estimation in the method based on deep learning. Although the radial profiles of velocity dispersions (σ) of GCSs can be self-consistently considered in the standard method based on the Jeans equation, the rotation amplitudes of GCSs and their radial and azimuthal dependencies are not properly included in the method. Also, the tracer mass estimator of Watkins et al. (2010) assumes spherically symmetric distributions of GCs and thus does not consider properly global rotation (along minor and major axes) of GCSs and its radial dependence. These suggest that the new mass estimation method based on deep learning can be promising, if a large number of 2D kinematics of GCSs can be used.

The purpose of this paper is thus to estimate the total mass of disk and elliptical galaxies by applying deep learning to the kinematics of GCSs of the galaxies. Since this is the very first paper on this topic, we try to demonstrate that the new method does work in the mass estimation using the synthesized two-dimensional (2D) maps of line-of-sight velocities (V) and velocity dispersion (σ) from numerical simulations of these galaxies with GCs. Accordingly, in this “proof-of-concept” phase of this project, we do not try to apply the developed method to real observations in the present study: it is our future study to estimate the total masses of galaxies by applying the method to real observations. We have also investigated the observational data of the globular

cluster system (GCS) in NGC 3115 Dolfi et al. (2020) : one of the authors in our paper is on Dolfi et al. (2020) (so that we can access to the data). However, we have found that the GCs in the galaxy are not distributed across the square field - we cannot have the reliable 2D map of GCS kinematics for the square region around the galaxy for a comparison with simulated square maps of GCSs. Since, we need the square map of GCS kinematics for the input data to CNNs, this is not an ideal situation.

There should be other datasets for other galaxies, but, it is beyond the scope of this paper to generate the square 2D maps of GCS kinematics using these data. Therefore, we would like to do this test in our forthcoming papers.

In this new method based on deep learning, we first need to generate a large number of pairs of (i) 2D maps of GCS kinematics and (ii) known total masses of galaxies (“labels”) from numerical simulations in order to train the convolutional neural networks (CNNs) using a training dataset. In this “supervised learning”, a large number of synthesized images of GCSs ($> 10^4$) are used in the present study.

We mainly investigate how accurately the CNNs can predict the total masses of galaxies whose 2D maps of GCSs are not used in the training phase of CNNs. We also investigate how the prediction accuracy can depend on the introduction of noise in the synthesized 2D maps of GCSs, because it is inevitable for spectroscopic estimation of V for GCs to have a certain degree of observational errors. We use the 2D kinematics maps of GCSs in isolated disk galaxies and elliptical galaxies formed from major merging of two disk galaxies with different orbital parameters. We adopt such idealized major merger models for elliptical galaxy formation, because this study is still in the proof-of-concept phase for the adopted new mass estimation method. We will use the 2D maps of GCSs from cosmological simulations of GCS formation in our future studies.

The plan of the paper is as follows. We describe (i) the models of disk and elliptical galaxies with GCS, (ii) a way to construct the 2D kinematic maps of GCSs, and (iii) the architectures of CNNs used in the present study in Section 2. We present the results of the predictions from CNN for disk and elliptical galaxies, in particular, the prediction accuracies of CNNs in the mass estimation in Section 3. Based on these results, we provide several implications of the present results in the context of mass estimation of galaxies using GCSs of galaxies in Section 4. We summarize our conclusions in Section 5. In this paper, we focus exclusively on the accuracy of prediction from CNNs in the mass estimation of galaxies (including dark matter) from GCS kinematics. Accordingly, we do not discuss other key issues related to the origin of GCSs in galaxies. Since we focus on the mass estimation of galaxies based on recent methods using GCS kinematics, we do not discuss other classic methods using the projected mass estimator, e.g., Bahcall & Tremaine (1981) and the total numbers of bright GCs, e.g., Prole et al. (2019).

2 THE MODEL

In this paper, we numerically examine the dynamical evolution of GCSs in isolated disk galaxies (“disk” models) and el-

lptical galaxies formed by major merging (“elliptical” models). We do not discuss the details of the physical characteristics of the disk and elliptical galaxies as we focus exclusively on the structures and kinematics of GCSs. The details of the evolution of the interstellar medium (ISM) are highly unlikely to influence the physical properties of GCSs because GCs are mostly located outside the gaseous and stellar disks of disk galaxies. We investigate isolated disk galaxy models with different rotation and different ratios of stellar bulges to the stellar disk of their GCSs. For merger models, we consider merging of two spiral galaxies with various bulge-to-disk-ratios and baryonic mass fractions. In our previous simulations, we investigated the chemodynamical evolution of disk and elliptical galaxies using our original simulation codes (i.e. Bekki & Shioya 1998; Bekki 2013). We use our original simulation code developed by Bekki (2013), though we do not investigate the evolution of gas, metals, and dust in the present paper.

2.1 Structure and kinematics of a stellar disk

The total masses of dark matter halo, gas disk, stellar disk, and bulge of a disk galaxy are assumed to have masses of M_h , M_g , M_s , and M_b , respectively. In this preliminary work, we only show the results of models with no gas ($f_g = M_g/M_s = 0$). The ratio of stellar bulge to stellar disk is denoted by a parameter f_b and is determined as M_b/M_s . The fundamental parameters in this investigation are M_h , f_{bary} , and f_b . We assume that the radial density profile of the dark matter halo is described as the Navarro, Frenk & White model suggested from Cold Dark Matter simulations in order to describe the initial density profile of dark matter halo in a disk galaxy Navarro et al. (1996). It is explained as:

$$\rho(r) = \frac{\rho_0}{(r/r_s)(1 + r/r_s)^2}, \quad (1)$$

where ρ_0 is the characteristic density of a dark halo, r is the spherical radius and r_s is defined as the scale length of the halo. The ratio of r_{vir} and r_s ($c = r_{\text{vir}}/r_s$) is known as c -parameter, where r_{vir} is known as the virial radius of a dark matter halo. The value of r_{vir} for a given dark halo mass (M_{dm}) is chosen by using the $c - M_h$ relation for $z = 0$, e.g., Neto et al. (2007).

The Hernquist density profile represents the bulge of a disk galaxy. This bulge of disk galaxy has a scale-length of $R_{0,b}$ and size of R_b . The bulge is supposed to have radial and isotropic velocity dispersion which are explained by Jeans equation for a spherical system. The value of bulge-to-disk ratio ($f_b = M_b/M_d$) for a disk galaxy ranges from 0 (pure disk galaxy) to 4 (bulge-dominated). The ‘Milky Way-type’ models are those with $f_b = 0.17$ and $R_b = 0.2R_s$, where R_s is the stellar disk size of a galaxy. We use the mass-size scaling relation which is given by $R_b = C_b M_b^{0.5}$. From this relation, R_b for a given M_b can be determined. The value of C_b is determined so that R_b can be 3.5 kpc for $M_b = 10^{10} M_\odot$ (corresponding to the mass and size of the Milky Way’s bulge).

The vertical (Z) and radial (R) density profiles of the stellar disk are proportional to $\exp(-R/R_0)$ having scale length $R_0 = 0.2R_s$ and $\text{sech}^2(Z/Z_0)$ with scale length $Z_0 = 0.04R_s$ respectively. The model we use for our study

Table 1. Description of the basic parameter values for the fiducial model for merging of two disk galaxies

Physical properties	Parameter values
Total halo mass (galaxy)	$M_{\text{dm}} = 1.0 \times 10^{12} M_\odot$
DM structure (galaxy)	NFW profile
galaxy virial radius (galaxy)	$R_{\text{vir}} = 245$ kpc
c parameter of galaxy halo	$c = 10$
Number of GCs in a GCS	$N_{\text{gc}} = 200$
Rotational energy fraction of a GCS	$f_{\text{rot}} = 0.0$
Stellar disk mass	$M_s = 6.0 \times 10^{10} M_\odot$
Stellar disk size	$R_s = 17.5$ kpc
Gas disk size	$R_g = 17.5$ kpc
Disk scale length	$R_0 = 3.5$ kpc
Bulge mass	$M_b = 10^{10} M_\odot$
Bulge size	$R_b = 3.5$ kpc
Mass resolution	$5.0 \times 10^4 M_\odot$
Size resolution	175 pc
Mass-ratio of two spirals in a merger	1.0
Initial distance of two spirals in a merger	140 kpc
Circular velocity factor of a merger	$f_v = 0.45$
Star formation	Not included
Chemical evolution	Not included
Dust evolution	Not included

has $R_s = 17.5$ kpc. The initial radial and azimuthal velocity dispersion are assigned to the disc component using the epicyclic theory with Toomre’s parameter, $Q = 1.5$, along with the rotational velocity produced by the gravitational field of the disk. The vertical velocity dispersion at a given point is set to be half the radial velocity dispersion at that point.

The total number of particles in a fiducial model with $f_b = 0 : 167$ is 1016700 and it depends on f_b . The mass resolution is $1.2 \times 10^4 M_\odot$ in all models of the current study. The gravitational softening length for every component is decided by the size of distribution and a total number of particles in each component (R_s and r_{vir}). It is set to be 320 pc, which is much finer than 1 – 2 kpc spatial resolutions used for the image analysis in this study.

These spatial and mass resolutions are not particularly high, mainly because we have to run numerous models for the limited amount of computing time allocated for this project. We believe that the adopted resolutions are good enough to construct the CNNs (later described) and analyze the image data from simulations.

2.1.1 Globular cluster systems

We briefly discuss the model as we use the same model for GCSs as used in Bekki et al. (2005). The GCS in a disk galaxy is supposed to have a radial density profile of $\rho(r) \propto r^{-3.5}$. Therefore, we assume that a GCS in a disk has radial density profile given by following equation:

$$\rho(r) = \frac{\rho_{\text{gc},0}}{(a_{\text{gc}}^2 + r^2)^{1.75}}, \quad (2)$$

where r is the spherical radius, $\rho_{\text{gc},0}$ is the central number density of the GCS, and a_{gc} is the scale length of the GCS.

This $\rho_{\text{gc},0}$ is defined according to the a_{gc} . In this study, we do not distinguish between metal-poor and metal-rich GCSs, though such two different GC populations are considered in Bekki et al. (2005). Therefore, we adopt a single value of $a_{\text{gc}} = 0.3R_d$ (~ 5 kpc for a Milky Way-type disk

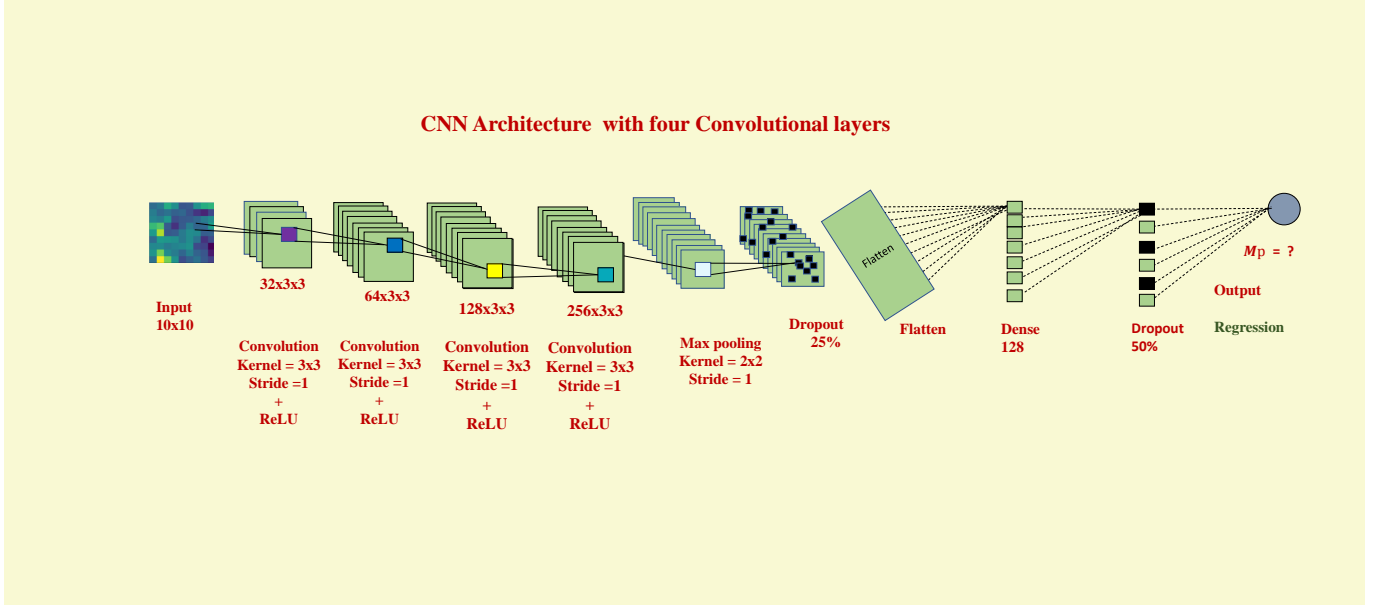


Figure 1. The adopted architecture of our original CNN with four convolutional layers followed by max-pooling layer, dropout and dense layers and a linear output layer. The details of the architecture are explained in the main text.

galaxy) for a GCS. This adopted value is consistent with the observed GC distribution of the galaxy. The cut off radius (R_c) is set to be $3R_d$ for GCSs (~ 50 kpc for a Milky Way-type disk galaxy). This is a radius beyond which no GC particles are initially allocated.

The GCS in a disk is supported by both rotation velocity and velocity dispersion. This velocity dispersion is assumed to be isotropic. We introduce a parameter f_{rot} that describes the ratio of total rotational energy (T_{rot}) of a GCS to its total kinetic energy (T_{kin}):

$$f_{\text{rot}} = \frac{T_{\text{rot}}}{T_{\text{kin}}}. \quad (3)$$

We assume that each GC is rotating around the spin axis of its host galaxy (the z -axis) and the above f_{rot} determines its rotational velocity. In order to estimate the rotational velocity of each GC, we take the following steps.

We first evaluate the 3D velocities of a GC particle from the gravitational potential at the position of dynamical equilibrium. This is a position where velocity dispersion at each GC should be the same as that for dark matter. We then add the rotational velocity to the GC and reduce the 3D velocities so that f_{rot} can be the adopted value. The total number of GCs in a disk galaxy is 200.

2.1.2 Orbital configurations of galaxy merging

The orbits of the two disks are initially set to be in the x - y plane in all the merger simulations with different mass-ratios of two disks (m_2). The distance between the centers of mass of the two disks is $[4 - 8]R_d$ for all models. The relative velocity of the two galaxies is $v_c * f_v$, where v_c is the circular velocity at the initial distance and f_v is the circular velocity factor (f_v) ranging from 0.05 (highly radial) to 1.0 (circular orbit). The GCSs of merger remnants in the models with larger f_v can show higher degrees of global rotation (i.e., More angular momentum in the GCSs), because the initial

two disk galaxies can have larger orbital angular momentum. On the other hand, the models with small f_v can have more radial orbital of GCs and lower intrinsic angular momentum in GCSs. Therefore, the diverse kinematics in GCSs can be seen in these models with different f_v .

θ_i denotes the spin of each galaxy in a merger, where the subscript i identifies each galaxy. Here, θ_i is the angle between the vector of the angular momentum of the disk and the z -axis. We change these angles for the two disks randomly. The azimuthal angle ϕ is measured from the x -axis to the projection of the angular momentum vector of the disk onto the x - y plane, and this is set to be 0 for the two disks because this is not an important parameter in the present study. The time when the progenitor disks merge entirely and reach the dynamical equilibrium is less than 20.0 in our units for most of the models, though it is longer for smaller m_2 .

2.1.3 Method to derive 2D kinematics maps of GCS

Figure 2 clearly explains the simulated galaxy is divided into 10×10 meshes with each mesh being investigated in terms of GCS kinematics. Moreover, we split the data to 80% vs 20% randomly for galaxy models too.

2.2 CNN Architecture

In the literature, CNNs have become the dominant deep learning approach for visual object recognition. It is used for image classification, object detection and segmentation. CNNs are not restricted to visual perception and are also successful at other tasks, such as voice recognition or natural language processing.

In the present study, we will use CNNs with the architectures similar to those used in our previous study for galaxies under ram pressure stripping and galaxy interaction for the regression problems of the present study Bekki

Table 2. A brief summary for the adopted architectures of CNNs and the results for dataset from (i) isolated disk models, (ii) elliptical galaxies models, and (i)+(ii).

Name	Number of images	Model image	CNN architecture	Training epochs	Accuracy (One-Channel)	Accuracy (Two-Channel)
DL1	100,000	disk galaxy	2 convo	1000	0.937	0.965
DL2	80,000	merger	2 convo	1000	0.972	0.980
DL3	200,000	disk + merger	2 convo	1000	0.946	0.959
DL4	200,000	disk + merger	4 convo	1000	0.976	0.978
DL5(noise)	200,000	disk + merger	4 convo	1000	0.809	0.812

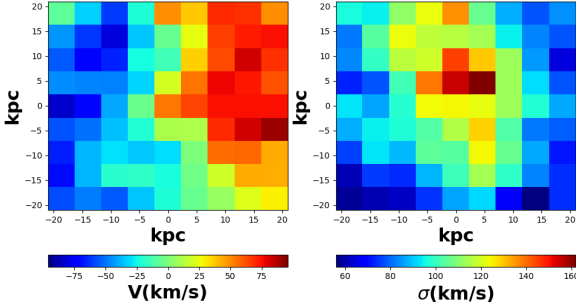


Figure 2. 2D maps of line-of-velocity (V , left) and velocity dispersion (σ , right) in the isolated disk model with global rotation in its GCS. The maps are derived within $R < 1.2 R_d$, where R_d is the initial size of the stellar disk in this model.

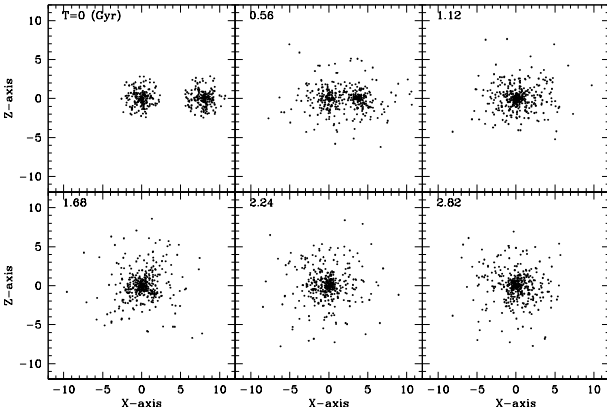


Figure 3. Time evolution of the projected distribution of GCs onto the $x-z$ projection (the orbital plane of the merger) in the fiducial merger model with $f_v = 0.45$ and $N_{gc} = 200$. Each dot is a GC, and the scale is given in simulation units (17.5 kpc).

et al. (2019) Bekki et al. (2019) Diaz et al. (2019) Cavanagh & Bekki (2020). We also use a CNN that is newly developed for the purpose of more accurate predictions of total masses of galaxies from GCSs.

The CNN network that we used for our model is summarized in Figure 1. In the following subsections, we describe the overall architecture of our CNN model.

2.2.1 Convolutional layers

The architecture initially consists of two convolutional layers. Neurons in the first convolutional layer are only connected to pixels in their receptive fields. Similarly, each neu-

ron in the second convolutional layer is connected only to the neurons in the receptive field of the first convolutional layer. This architecture enables the network to focus on low-level features in the first hidden layer, then combine them into higher-level features in the next hidden layer Géron (2017).

The first convolutional layer filters the $(10 \times 10 \times 1)$ input image with 32 filters of size $(3 \times 3 \times 1)$ having stride of length 1 (both horizontally and vertically) and “valid” padding. Here, the stride is a distance between two receptive fields. In convolutional layer, choosing an appropriate number of filters is significant for feature detection. We can start any neural network with filter range $[32, 64, 128]$ in the input layers and increasing their size to $[256, 512, 1024]$ in deeper layers Géron (2017).

The convolutional layers require another parameter which is kernel size. There are various kernel sizes available $(1, 1)$, $(2, 2)$, $(3, 3)$, $(5, 5)$ and $(7, 7)$. Since our input size for the images is (10×10) pixels, we prefer to use the kernel size of (3×3) . If we have a larger image, then we can use larger kernels. Also encouraged by the architecture of VGGNet, we decided to use the kernel size of (3×3) Simonyan & Zisserman (2014). Similarly, the second convolutional layer in our network has 64 filters of the same kernel size (3×3) with stride (1×1) . The number of parameters in the first and second convolutional layer are 320 and 18,496, respectively.

Moreover, we used our convolutional layers with ReLU activation function, because ReLU trains network several times faster as compared to the tanh activation function (Krizhevsky, Sutskever & Hinton 2017). The study showed that a four-layer CNN with ReLUs attained 25% training error rate on CIFAR-10 (i.e. it took 6 times less time to train than a comparable network with a tanh activation function) Krizhevsky et al. (2017). Therefore, we decided to select ReLU as an activation function with each convolutional layer to save computing time.

2.2.2 Pooling layers

Since, max-pooling layer in CNN architecture offers stronger translation invariance than average pooling, and it requires slightly less work to compute. Therefore, max-pooling layers are now more commonly used as compared to average pooling layers. Hence, we decided to use only one max-pooling layer with (2×2) and stride of 1 (both horizontally and vertically) in order to get the best features and reduce computational complexity. It is used to reduce the input shape further, and the network does not learn anything from this layer. Therefore, the number of parameters in max-pooling remains 0.

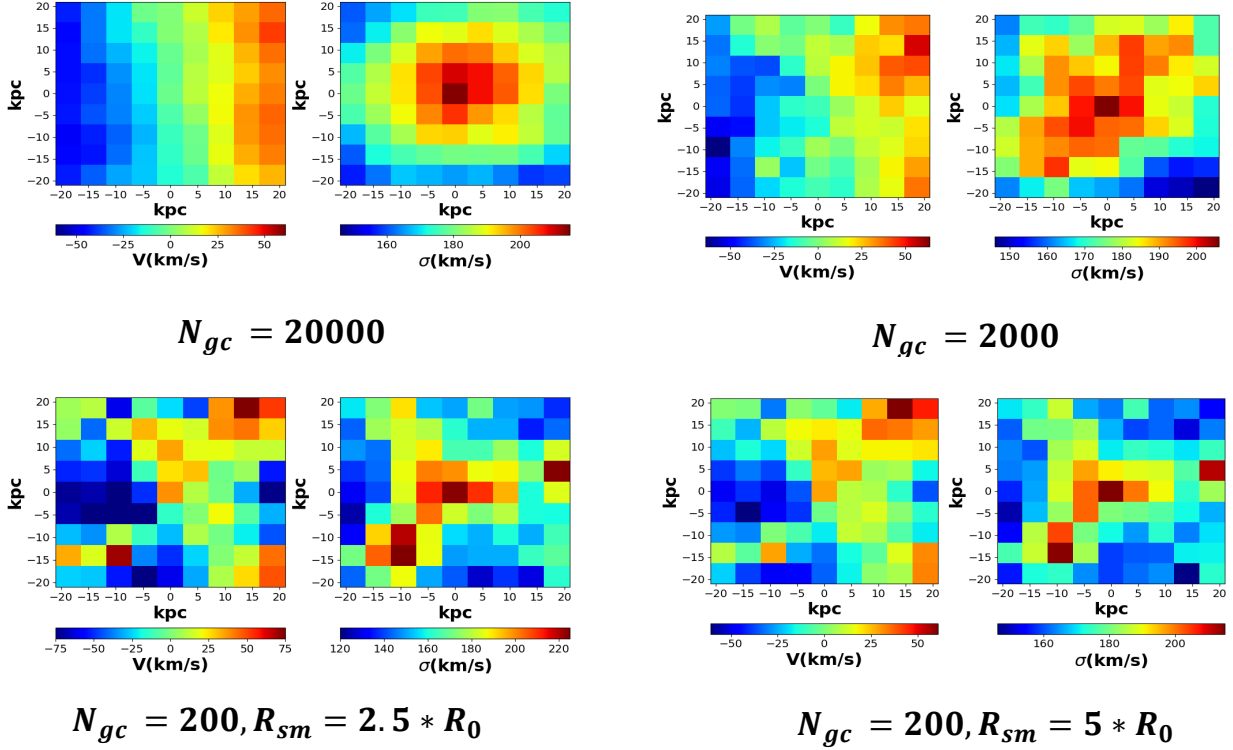


Figure 4. 2D maps of V and σ for merger models with $N_{gc} = 20000$ (upper left), $N_{gc} = 2000$ (upper right), $N_{gc} = 200$ and $R_{sm} = 2.5 \times R_0$ (lower left) and $N_{gc} = 200$ and $R_{sm} = 5 \times R_0$. Here R_0 is the scale length of the initial stellar disk.

2.2.3 Dropout

Dropout has proven to be highly successful and is reported to give 1-2% accuracy improvement in results Hinton et al. (2012). The dropout technique consists of producing zero output for each hidden neuron with some probability. We use dropout with a fully connected layer with probability 0.50. The purpose of this layer is to help our network generalize and not to over-fit. Neurons from the current hidden layer with probability p will randomly disconnect from neurons in the next hidden layer so that the network has to rely on the existing connections. The hyper-parameter p is called the *dropout rate*, and it is typically set to 50%. Since dropout just removes the nodes that are below the mentioned weights, the number of parameters in the dropout layer remains zero. At testing phase, we simply use the connection weights that have been learned from the training process.

In our architecture, we used two *dropout* layers; one is on top of max-pooling layer while the other is on top of the dense layer. We set our max-pooling layer to have a *dropout rate* of 25%, and a dense layer with 128 neurons having a dropout rate of 50%.

2.2.4 Output layer

The last layer of our CNN architecture is the output layer. We do not use any dropout layer on the output layer. The fully connected layer, in the end, contains 73,856 parameters. A “linear activation function” is added at the last

layer to the network. The output of this layer is the prediction value itself. In our case, its output is the mass of the dark matter M_p which is normalized to 0-10 value. We have converted it into Msun for the output.

2.2.5 CNN with four convolutional layers

One of the most critical choices in network design was the number of convolutional layers. It was noticed that successive 2D convolutional layers have the effect of transforming input to extract increasingly high-level representation, at the expense of spatial resolution Hariharan et al. (2017). In our research, we tested our CNN with a different number of convolution layers, to investigate the trade-off between extracting higher-level features and preserving spatial resolution. Initially, we started with two layers and tested our model on one-channel and two-channel data. Then, motivated by AlexNet’s architecture Krizhevsky et al. (2012), we put four convolution layers directly on top of each other. Table 2 and Table 3 show the results with both architectures. We found that the accuracy of our model increased by adding more convolution layers. Therefore, our final model contains four convolutional layers on top of each other as shown in Fig. 1.

The third convolutional layer has 128 filters with kernel size 3×3 followed by next convolutional layer having 256 filters with the same kernel size 3×3 . The total number of parameters in the architecture with two convolutional layers is 92,930. However, the number of parameters significantly

increases to 420,994 in case of four convolutional layers architecture.

2.2.6 Performance comparison measures

We have calculated errors to compare the performance of our model on one-channel and two-channel data using error density plots, given by the following equation:

$$E_i = \frac{(M_p - M_c)}{M_c} \quad (4)$$

where, M_p and M_c represent the predicted and actual mass of dark matter, respectively.

Moreover, it is also necessary for our research to look at cumulative distribution plots in order to compare the performance of one-channel and two-channel data. We use the absolute values of errors to plot cumulative distribution plots as given in the following equation:

$$|E_i| = \frac{|M_p - M_c|}{|M_c|} \quad (5)$$

Additionally, we use the well-established Root Mean Square Errors (RMSEs) and Mean Absolute Errors (MAES) as metrics for evaluating model performance. We have also used accuracy of the model in order to compare performance of CNN for images from different galaxies. M_c and M_p are the normalized values 0-10. We converted them into Msun for the output, but, the real DM masses are used for the accuracy estimation. Moreover, the number of bins used for accuracy estimation is 20. In the following section, we will describe our significant results of estimation of dark matter mass using the proposed CNN architecture.

3 RESULTS

We first briefly show the 2D kinematics maps of GCs in the fiducial merger model with different N_{gc} , because we need to demonstrate how the present results can depend on N_{gc} in Section 3.1. Then we describe the results of the CNN-based mass from GCSs in disk galaxies using 100,000 images dataset (e.g, 2D maps of σ and V) in Section 3.2. Table 2 describes the number of images and the model parameters for CNNs. For these disk galaxy models, we divide the images into 80,000 for training CNNs and 20,000 for testing. We also describe the results for the elliptical galaxy models (i.e., galaxy mergers) with 80,000 images in Section 3.3. We then show the results for the combined dataset from disk and elliptical galaxy models in Section 3.4. For these results, the testing data are different from the training one, but both are generated from the same galaxy models. In Section 3.5, we test the CNN trained by these images for the totally unknown dataset that is not used in training CNNs. Thus we can check the prediction accuracy of our CNNs in a more stringent manner. In Section 3.6, we demonstrate how the obtained results depend on the CNN architectures by comparing the prediction accuracies between different CNNs.

3.1 2D Kinematics maps for GCSs

We generate 100 images of the GCS in a galaxy viewed from 100 angles. Therefore, one galaxy has 100 different images. For example, DL1 model sequence has 100,000 images

(training data set), which means $100,000/100 = 1000$ different GCSs (galaxies) are used. Since the number of GCs are quite different in different elliptical galaxies, we investigate the details of 2D maps for the present study to investigate how the 2D maps of V and σ depend on the number of GCs (N_{gc}). Fig. 4 describes the 2D maps for the fiducial merger model with different $N_{gc} = 200, 2000$ and 20000 and different Gaussian smoothing length of $R_{sm} = 2.5R_0$ and $5.0R_0$ for $N_{gc} = 200$. This demonstrates that (i) global rotation of this GCS can be clearly seen in all four models, i.e., even in the model with a low GC number and (ii) the radial gradient of σ , which is a key in the mass estimation of galaxies, can also be clearly observed. These details of GCS kinematics, such as radial gradients of σ and V profiles, are the characteristic features that our CNNs can capture to estimate the total masses of galaxies.

However, the random noise due to a small number of GCs per pixel can be more remarkable for the models with low GC numbers. It is a key question in this study whether the trained CNN can predict accurately the total masses of galaxies with low GC numbers (i.e., with noisier 2D maps). As shown in the subsequent subsections, even our CNNs trained by images from GCSs with $N_{gc} = 200$ can accurately predict the total masses of galaxies from GCS kinematics. This implies that noisy images do not greatly prevent CNNs from learning the characteristic features of GCS kinematics that depend on galaxy masses. Other problems related to observational noise in spectroscopic determination of V and σ will be discussed in Section 4.

3.2 CNN prediction of disk galaxies

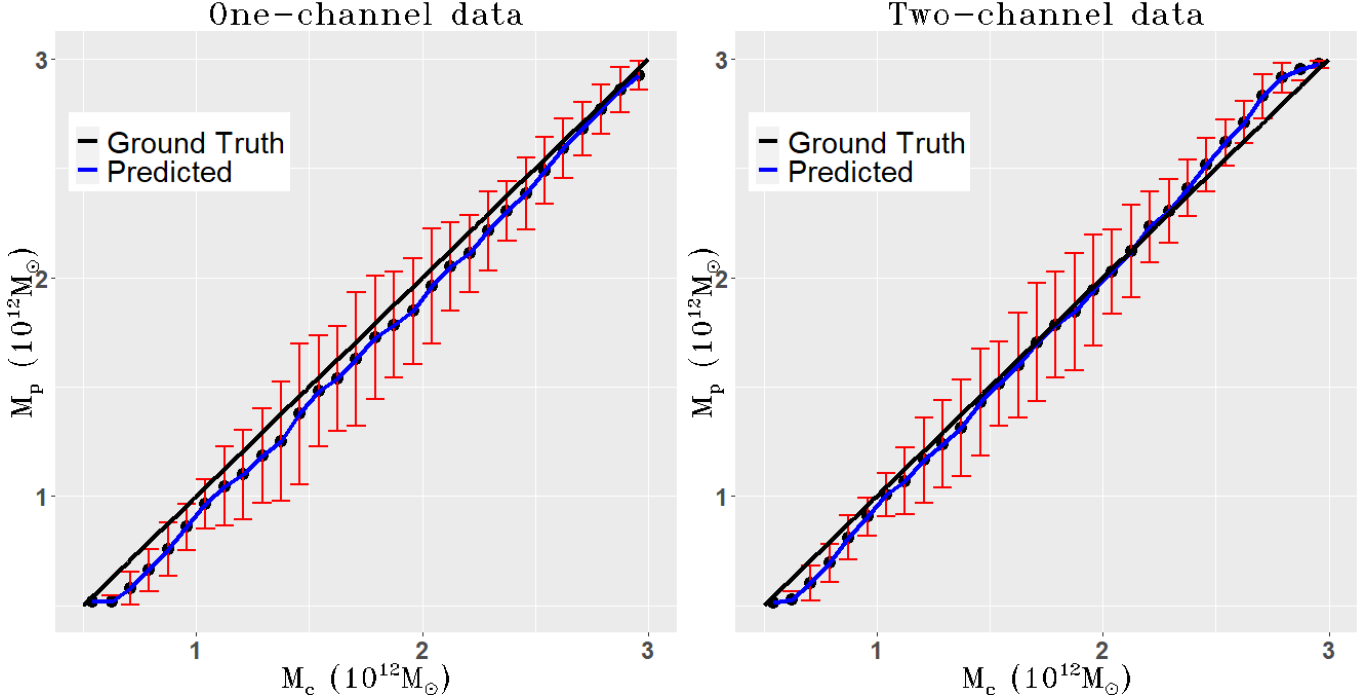
In the first set of experiments, we have selected 100,000 images from disk galaxies, 80% of images were randomly selected for training while rest of 20% were dedicated for testing the performance of our network. We have trained our CNN for 1000 epochs for disk galaxies models and for others in this study, because 1000 epochs are enough for the prediction accuracy to become very high (more than 95%). From Table 2, the model's accuracy for one-channel and two-channel data for disk galaxies are 0.937 and 0.965, respectively. This indicates that the CNN trained by two-channel data has a higher accuracy as compared to one-channel data. This is mainly because the CNN trained by two-channel data can properly consider global rotation (i.e., rotational energy of self-gravitating systems) in the mass-estimation.

Furthermore, Fig. 5 presents a detailed comparison between the predicted galaxy mass and the correct one ("ground truth") for disk galaxies. In this Fig. 5, M_c on the x-axis represents correct dark matter masses and the y-axis indicates predicted dark matter mass in disk galaxy images. The error bar in each mass bin represents the overall mean and standard deviation for the predicted values of total galactic masses. The black line indicates where $M_c = M_p$ and the blue one connect the average of the predicted mass in each bin in Fig. 5. This clearly demonstrates that the CNN can accurately predict the total mass of galaxies for a wide range of galaxy masses, though the standard deviation is not very small.

It is observed from Fig. 5 that the two-channel (velocity dispersion σ , and line-of-sight velocity V of GCs) predictions are better as compared to one-channel (velocity dis-

Table 3. Summary of results for CNN model used for disk, merger and disk + merger galaxies.

Name	Images	Model Image	MAE (One-channel)	MAE (Two-channel)	RMSE (One-channel)	RMSE (Two-channel)
DL1	100,000	disk galaxy	0.571	0.404	0.833	0.707
DL2	80,000	merger	0.265	0.188	0.357	0.239
DL3	200,000	disk + merger	0.501	0.367	0.733	0.595
DL4	200,000	disk + merger	0.288	0.275	0.539	0.51
DL5(with noise)	200,000	disk+merger	2.722	2.835	3.234	3.408

**Figure 5.** Predicted vs correct dark matter mass within disk galaxies for one-channel (left) and two-channel data (right). Here one-channel (two-channel) means that only σ data (both σ and V data) is used in the CNN-based prediction. M_c on the x-axis represents the correct value of dark matter mass, and M_p on the y-axis represents predicted dark matter mass. Error bars in the plot represent overall mean and standard deviation of the dark matter masses within disk galaxies. The Black line indicates $M_p = M_c$, and the blue line represents the predicted mass values for dark matter within disk galaxies. **The number of bins used is 20.**

person σ) predictions as the error bars are small in case of two-channel data. For an idealistic behavior, the error-bar plot should have points symmetrically distributed around the 45-degree straight line. The two plots in Fig. 5 show absolute symmetry. Hence, the accuracy of 93.7% and 96.5% are proved through these plots.

Moreover, Table 3 gives information about MAEs and RMSEs for one-channel and two-channel data for different galaxy models. Table 3 shows RMSEs for one-channel and two-channel data for disk galaxies are 0.833 and 0.707, respectively, and MAEs for one-channel and two-channel data are 0.571 and 0.404, respectively. This means model with two-channel data for disk galaxies performs better than the model with one-channel data as the values of RMSEs and MAEs for the model with two-channel data are smaller than the model with one-channel data. These results again confirm that global rotation of GCSs should be considered for more accurate mass estimation of galaxies.

Furthermore, Fig. 6 presents the error distribution plot for one-channel and two-channel data for disk galaxy images. It is a line plot for histogram. Since, the intervals on the x-axis are very fine, the plot will look cluttered, that is why

it is plotted as a line. It can be observed that E_i on the x-axis represents the errors calculated from Equ. (4) using the predicted values of total galaxy mass and the ground truth (i.e., correct mass). The y-axis represents the number of errors per each bin. Since the line of two-channel data (orange curve) near the zero is higher as compared to one-channel data (blue curve) in Fig. 6, we can say that the model with two-channel data gives better predictions in comparison to the model with one-channel data in case of disk galaxies.

The performance of models with one-channel and two-channel data can be quantified reasonably well by using the cumulative error distribution graph shown in Fig. 7. In this figure, $|E_i|$ on the x-axis represents the absolute values of errors calculated from Equ. (5) using the predicted values of galaxy mass and the ground truth. The y-axis shows $N(E < |E_i|)$, i.e., the total number of images with the predicted E less than a certain value (E_i). From Fig. 7, the model with two-channel data (orange curve) shows that around 45% of predicted dark matter mass has less than 5% of errors. On the other hand, the model with one-channel data (blue curve) in the same Fig. 7 shows more than 30% of predicted dark matter mass has less than 5% of errors.

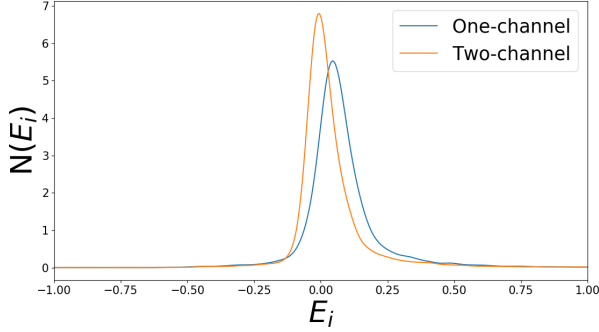


Figure 6. Distribution of errors E_i in the mass estimation of dark matter halos within disk galaxies: one-channel (blue) and two-channel (orange). The ways to derive E_i and $N(E_i)$ are described in the main text.

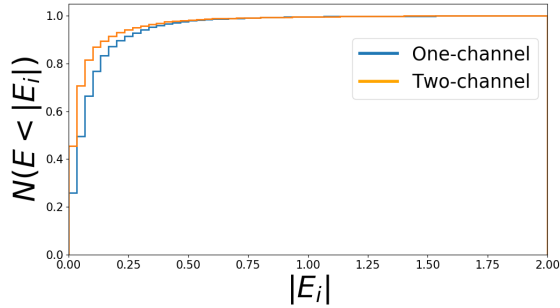


Figure 7. Cumulative error distribution graph for dark matter mass of disk galaxies in terms of physical units for one-channel (blue) and two-channel data (orange). Here, $|E_i|$ on the x-axis represents the absolute value of errors. The y-axis represents the normalized number of images per each $|E_i|$ bin.

Hence, it is clear that our CNN model gives better predictions, if the CNN is trained using two-channel data rather than one-channel data for disk galaxies.

3.3 CNN prediction for elliptical galaxies

Our CNN is also trained by using 64,000 images from elliptical galaxies formed from major merging with different orbital parameters and disk inclination angles with respect to their orbital planes. The predictions from our CNN for the 16,000 (20% of data) testing images are analyzed and summarized in Figs. 8-12. Table 2 shows that the model accuracy for elliptical galaxies using one-channel and two-channel data are 0.972 and 0.980, respectively, which is much better than our results for disk galaxies. The reason for this is as follows. The GCSs in disk galaxies are rotating along the z -axis (i.e., the disk planes) so that global rotation can be properly captured by our CNN if the galaxies are viewed edge-on. Therefore, the two-channel predictions by our CNN work very well for such viewing angles. However, if the galaxies are viewed from face-on, then the prediction accuracy becomes worse, because the rotation factor in the mass estimation cannot be properly considered by the CNN. For the merger case, such viewing effects are less important so that the mass estimation by our CNN can be more accurate.

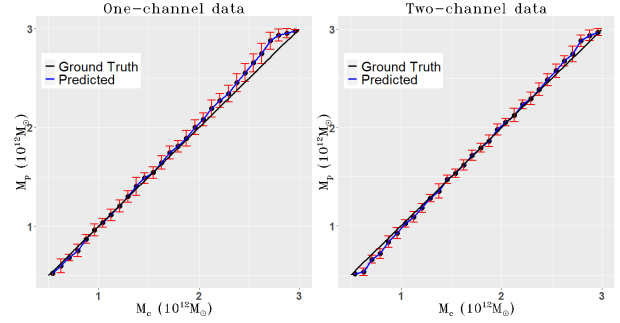


Figure 8. Predicted vs correct dark matter mass within elliptical galaxies for one-channel (left) and two-channel data (right).

The model with two-channel data performs better than the model with one-channel data for elliptical galaxies as well, as accuracy is higher in case of two-channel data.

Fig. 8 clearly demonstrates that our CNN's predictions are quite accurate for most images from elliptical galaxies with different total masses. This confirms that our CNN model gives better predictions in case of mergers as compared to isolated disk galaxies. The error-bar plot shows idealistic behavior as all the points symmetrically distributed around the 45-degree straight line. Hence, the accuracy of 97.2% and 98.0% for one-channel and two-channel respectively can be clearly observed in Fig. 8. The two-channel predictions in this case again look better as compared to one-channel predictions, which is totally consistent with the results from other models in this study. This again strongly suggests that rotational properties of GCSs should be properly considered in the mass estimation of elliptical galaxies formed by major merging.

Table 3 shows RMSEs for one-channel and two-channel data for elliptical galaxies are 0.357 and 0.239 respectively, and MAEs for one-channel and two-channel data are 0.265 and 0.188 respectively, for elliptical galaxies. Again in both cases, the model with two-channel data has smaller error values as compared to one-channel data (i.e., more accurate predictions in two-channel). Moreover, these error values are almost half of the error values of disk galaxies, which confirms that our CNN performs better in case of elliptical galaxies as compared to disk galaxies. Fig. 10 shows that (i) more than half of predicted total galaxy mass has less than 5% of errors and (ii) the two-channel CNN model gives better predictions in the elliptical galaxies too.

3.4 CNN prediction for combined data (Disk+elliptical galaxies)

We train our CNN using 160,000 of 200,000 images from GCSs in disk and elliptical galaxies (80% of data) and then test the CNN by the remaining 40,000 images (20%). We do this test in order to confirm that our CNN can accurately predict the total masses of galaxies for different types of galaxies. Figs. 11 and 12 demonstrates that (i) the combination of images from two different types of galaxies do not influence the prediction accuracy in the CNN-based mass estimation, (ii) the prediction accuracy does not depend on the mass of galaxies (i.e., smaller dispersion in each mass bin), (iii) the CNN can predict the total mass of galaxies with less than 25% errors for most images, and (iv) two-

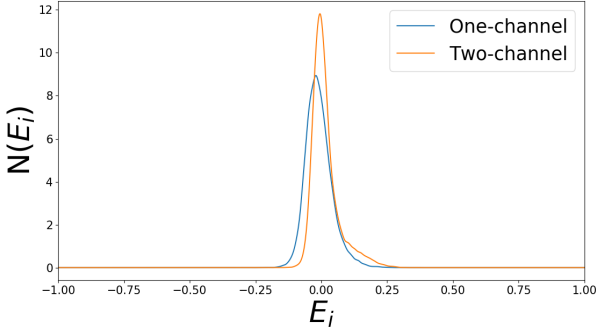


Figure 9. Distribution of errors E_i in the mass estimation of dark matter halos within elliptical galaxies: one-channel (blue) and two-channel (orange).

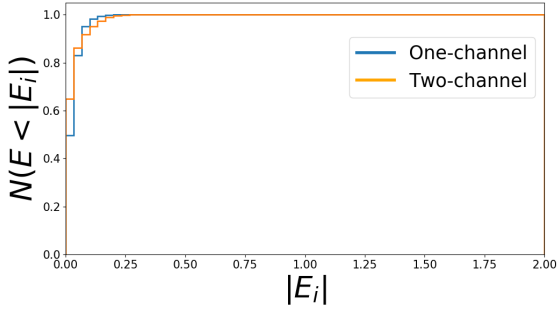


Figure 10. Cumulative error distribution graph for dark matter mass of elliptical galaxies in terms of physical units for one-channel (blue) and two-channel data (orange).

channel CNN model can more accurately predict the total galaxy masses than one-channel CNN model.

Table 2 shows that the accuracies for one-channel and two-channel dataset for this combined model are 0.946 and 0.959 respectively. These accuracies are higher than the accuracies from disk model but less than merger models. Table 3 shows that RMSEs for one-channel and two-channel data are 0.733 and 0.595 respectively, and MAEs for one-channel and two-channel data are 0.501 and 0.367 respectively. This better performance can be clearly seen in Fig. 12 and in Fig. 13. In Fig. 13, our CNN model with two-channel data (orange curve) shows around 45% of the all images have less than 5% of errors. On the other hand, the CNN model with one-channel data (blue curve) shows that about 30% of the images have less than 5% of errors: the better performance of the two-channel CNN is confirmed again.

3.5 CNN prediction for completely unknown data

Here we apply our CNN trained by the combined dataset (disk + elliptical galaxy models) to completely unknown dataset that is not used at all for training the CNN. This means that the galaxy models are not used at all in the testing data sets. This is a more stringent test for our CNN, because these structures and kinematics of the simulated GCSs in the unknown dataset can be significantly different from those used for training the CNN. The results for this are described in Figs. 14, 15 and 16. Fig. 14 confirms that

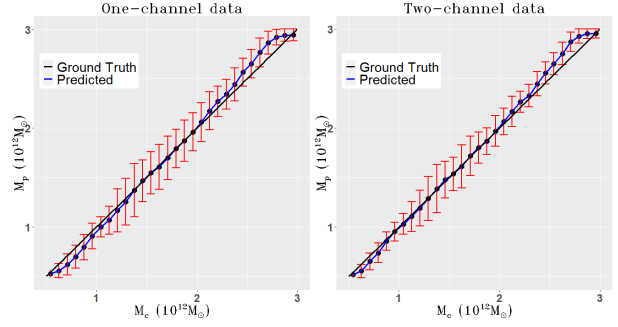


Figure 11. Predicted vs correct dark matter mass within disk and elliptical galaxies for one-channel (left) and two-channel data (right).

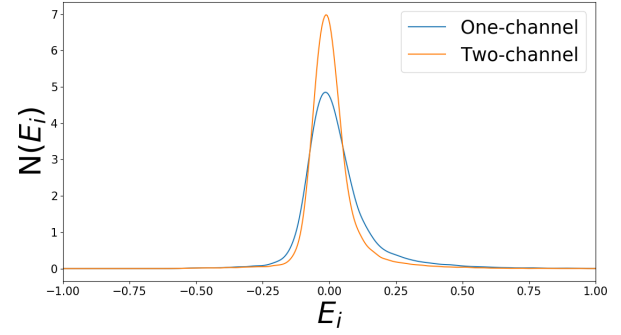


Figure 12. Distribution of errors E_i in the mass estimation of dark matter halos within disk and elliptical galaxies: one-channel (blue) and two-channel (orange).

our CNN performs pretty well even if we apply the CNN to an entirely unknown dataset. This is a very promising result, which implies that our CNN will be able to be applied to real observational dataset that is not fully covered by the present simulations. Better performance in the two-channel CNN prediction can be clearly seen in Fig. 15 and Fig. 16.

3.6 Predictions from a CNN with four convolutional layers

The results from our original CNN with only two convolutional layers are described in the preceding subsections. Here

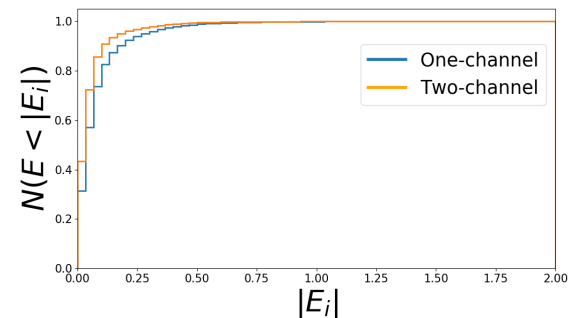


Figure 13. Cumulative error distribution graph for dark matter mass of disk and elliptical galaxies in terms of physical units for one-channel (blue) and two-channel data (orange).

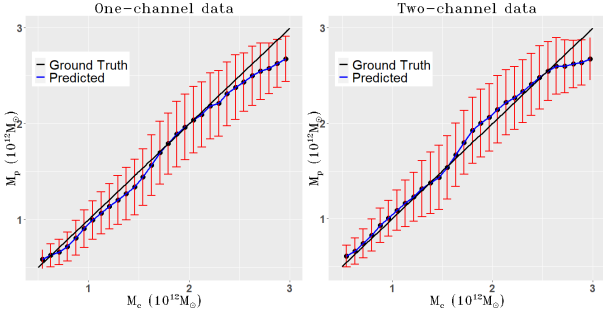


Figure 14. Predicted vs correct dark matter mass within completely unknown galaxies for one-channel (left) and two-channel data (right).

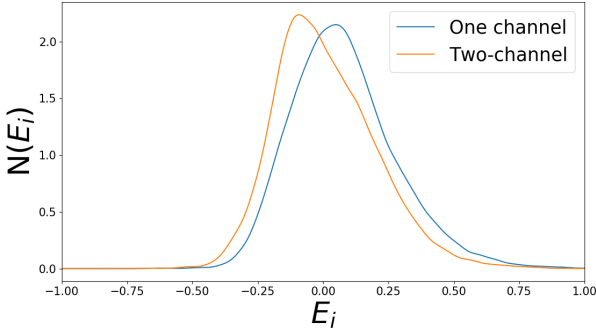


Figure 15. Distribution of errors E_i in the mass estimation of dark matter halos within completely unknown galaxies: one-channel (blue) and two-channel (orange).

we describe the results from our other CNN with two additional convolutional layers that are designed to improve the prediction accuracy in the mass estimation of galaxies from GCS kinematic (see the CNN architecture in Fig. 1). Table 2 describes that the prediction accuracies for this CNN are 0.976 and 0.978 for one-channel and two-channel data respectively. Table 3 shows that MAEs for one-channel and two-channel data are 0.288 and 0.275, and RMSEs are 0.539 and 0.51 for one-channel and two-channel data respectively. It is clear that adding two layers in our CNN architecture results in an improvement of accuracy both for one-channel and two-channel dataset. However, we confirm that CNNs with more convolutional layers (e.g., 6 of them) cannot further improve the accuracy of prediction.

4 DISCUSSION

4.1 Advantages and disadvantages of the new method

We have demonstrated that the new method based on deep learning can predict the total masses of galaxies pretty well, though the number of images used for training CNNs is not huge (“like” be “in order of 10^6 samples”). The mean accuracy of the prediction can reach 98% (i.e., the predicted masses deviate from the true values by only 2%), which implies that the new method will be able to be applied to the kinematics of the observed GCSs. Furthermore, the better prediction accuracy for two-channel data (V and σ) implies

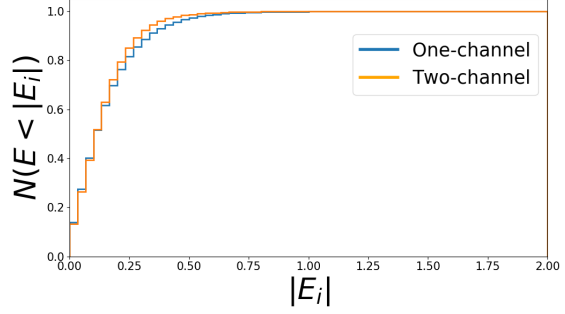


Figure 16. Cumulative error distribution graph for dark matter mass of completely unknown galaxies in terms of physical units for one-channel (blue) and two-channel data (orange).

that global rotation of GCSs needs to be incorporated into the mass estimation models for more accurate predictions of total masses in galaxies. This also implies that the total masses of galaxies with GCSs with higher amplitudes of global rotation, e.g., NGC 3115 Dolfi et al. (2020) can be better estimated by the present new method than others that only consider the radial profiles of σ for GCSs. We suggest that if the 2D kinematics of GCSs predicted from cosmological simulations of GC formation, e.g., Pfeffer et al. (2017) can be used to generate the synthesized 2D maps of GCS kinematics that can be input to CNNs, an even better mass estimator based on deep learning can be developed, because the predicted kinematics can be more diverse and more realistic than the synthesized images adopted in the present study.

The new method, however, has the following possible problems, which need to be solved in our future studies. First, the total number of GCs in a galaxy should be at least several tens to ~ 100 so that the 2D maps of V and σ with enough spatial resolutions (e.g., 10×10 pixels) can be constructed. This means that the new method cannot be properly applied to GCSs of less luminous galaxies like NGC 4564 with $N_{gc} = 27$ Alabi et al. (2016). If there is no GC in a significant number of pixels for less luminous galaxies, a large smoothing length need to be applied to the 2D maps so that smooth V and σ fields can be derived. However, such a large smoothing length would cause a significant reduction of the prediction accuracy in the mass estimation. Second, it is not so clear how sensitive the new mass estimation method is to the presence of substructures in GCSs. In the present disk and elliptical galaxy models with GCSs, the synthesized images do not show substructures clearly whereas some of the observed GCSs show substructures Alabi et al. (2016). This means that the training dataset should contain GCSs with substructures for more accurate predictions of total galactic masses in our future study.

Third, observational errors in the spectroscopic estimation of line-of-sight-velocities (V) for individual GCs can possibly introduce noise in the 2D maps of GCSs. If CNNs are trained by 2D images with such noise, then the prediction accuracy will be reduced significantly too. In order to investigate this issue more quantitatively, we add Gaussian noise manually to the image data and thereby investigate the performance of our CNNs. We add noise with mean zero and standard deviation of 0.04 to each pixel in this investigation.

This error correspond to spectroscopic errors of $\sim 5 \text{ km s}^{-1}$ for V and σ . The $\sim 5 \text{ km s}^{-1}$ error in each mesh corresponds to the observationally possible errors for radial velocities of GCs Dolfi et al. (2020). Therefore our adoption of this value is consistent with observations of GCSs. Since there can be a number of GCs in one pixel, it is not straightforward to convert observational errors for one GC into noise (errors) for the estimated V and σ for one pixel, this introduction of noise enables us to discuss this important issues in a quantitative manner. Fig. 17 represents the 2D map of the image without noise, with noise, and noise only. It is found that after adding noise to images, our model accuracy significantly drops from 0.976 to 0.809 for two-channel combined data from disk and elliptical galaxies (disk+merger). Moreover, RMSEs for one-channel and two-channel data for images with noise are 3.234 and 3.408, respectively, and MAEs for one-channel and two-channel data are 2.722 and 2.835, respectively. This means that our model still performs well on the dataset containing noise, though the prediction accuracy would become worse for noise of more than 10 km s^{-1} .

4.2 Toward the application of the new method to observations

Although we have developed the new mass estimation method based on deep learning, this work can be regarded as a proof-of-concept. In order to apply the new method to real observations, we need to (i) solve the above-mentioned three possible problems related to the implementation of the new method and (ii) significantly increase the number of synthesized images of GCSs not only from constrained simulations (like the present study) but also from cosmological ones. The above second point is crucial for our future work, because the simulated kinematics of GCSs from isolated disk galaxies and major mergers is quite limited and possibly could not represent a full range of the observed kinematics of GCSs with diverse rotation amplitudes and anisotropy parameters (i.e., tangentially or radially anisotropic).

The formation and evolution of GCSs in galaxies with different masses and types can involve various physical processes of galaxy formation (not just major merging and secular disk evolution modeled in this study). Therefore, it is ideal for our future study to generate the synthesized 2D kinematics of GCSs in galaxies from cosmological simulations that can model various physical processes of galaxy formation from the early universe. Since previous and recent cosmological simulations of GCS formation in galaxies have already predicted the kinematics of GCSs, e.g., Bekki et al. (2008) Pfeffer et al. (2017), it will be feasible for our future study to generate a large number of 2D kinematics maps of GCSs from these simulations, which will be input to CNNs for better prediction accuracies.

5 CONCLUSIONS

We have developed a new method by which we can estimate the total masses of galaxies including their dark matter halos from the kinematics of their GCSs. This new method is based on deep learning in which a large number of synthesized 2D maps of kinematics of GCSs from numerical simulations of galaxies with known total masses are used

to predict the total masses of galaxies. The new mass estimation method has involved the following two steps. In the first step of the method, we have trained a convolutional neural network (CNN) using a large number (more than 100,000) of synthesized 2D kinematics maps (“images”) of GCSs from simulated disk and elliptical galaxies with known total masses. Accordingly, the input data to a CNN is the large number pairs of (i) 2D kinematics maps of GCS and (ii) true (known) total masses of galaxies including dark matter.

In this supervised learning phase, either only 2D maps of velocity dispersions (σ) of GCSs (“one-channel”) or 2D maps of both σ and V (line-of-sight-velocities) of GCSs (“two-channel”) are used so that we can determine whether one-channel or two-channel prediction can be more accurate. This large number of images can cover a wide range of GCS kinematics with various degrees of global rotation and anisotropy parameters, though the present study possibly would not cover a full range of the observed GCS kinematics. In the second step of the method, we have applied the CNN to a completely unknown dataset to investigate whether or not the CNN can accurately predict the true masses of galaxies.

For disk galaxies, we have used 100,000 images of GCSs kinematics from different disk galaxies with different degrees of rotational kinematics in GCSs. We have used 80,000 images of GCSs kinematics for elliptical galaxies, and also combined these images from the two types of galaxies. In order to investigate how observational errors (represented as noise in pixels) can influence the prediction accuracy of the new mass estimation method, we have added Gaussian noise to the images from the combined dataset (disk+merger) with mean 0 and standard deviation of 5 km s^{-1} . Furthermore we have verified the prediction accuracy of our CNN using RMSEs and MAEs for each model. We have compared between different architectures of CNNs in terms of prediction accuracies and shown the results from the best CNN architecture in the present study. The principal results are as follows:

(1) Our new model based on our original CNN can predict the total masses of disk galaxies dominated by dark matter pretty accurately. The overall accuracy of the model trained by only 2D maps of σ of GCSs (one-channel data) is 93.7%. However, the accuracy of the model trained by 2D maps of V and σ (two-channel data) is improved by about 3%. We have observed MAE of one-channel data is 0.571 and for two-channel data, it is 0.404, which clearly demonstrate a very high prediction accuracy. Moreover, RMSEs for one-channel and two-channel data are 0.833 and 0.707, respectively. This implies that the model with two-channel data works better than one-channel data, as two-channel data has a smaller MAE. This is mainly because the rotation energy of GCSs can be properly considered in the mass estimation of galaxies including dark matter: this contribution from global rotation should be considered in the mass estimation.

(2) Our model can also accurately predict the total masses of elliptical galaxies including their dark matter. The observed accuracies for the model trained by one-channel and two-channel data are 97.2% and 98%, respectively. These accuracies are slightly better than our results for disk galaxies. The outcomes for RMSEs for elliptical galaxies

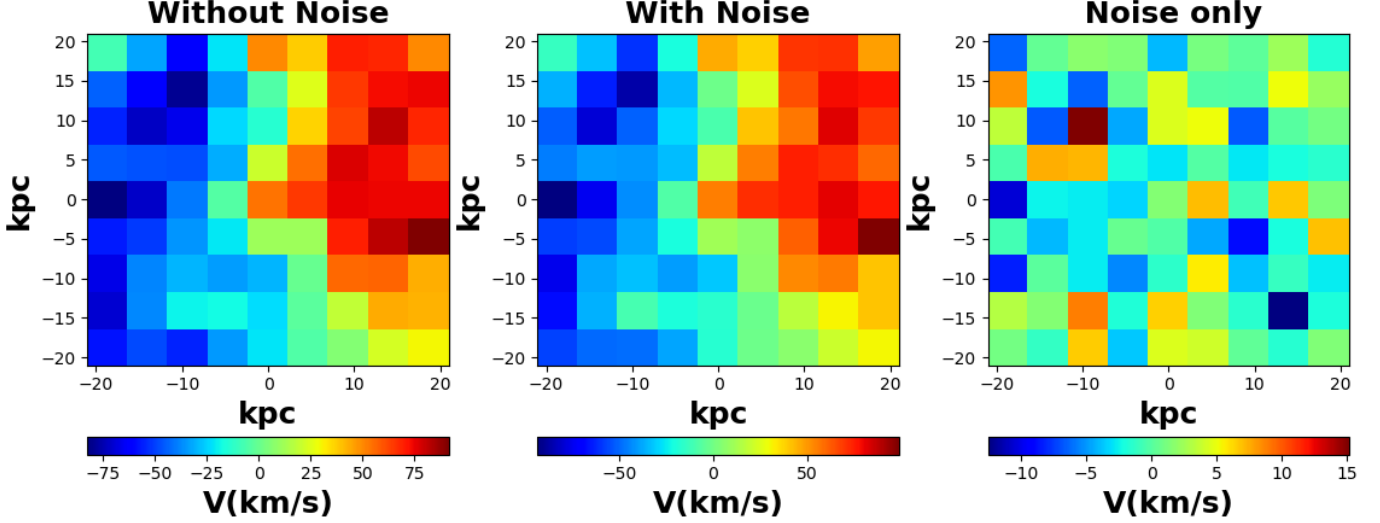


Figure 17. 2D map of V without (left) and with noise (middle) for the GCS of a isolated disk galaxy. Noise with the mean of 0 and the standard deviation of 0.04 (in simulation units, corresponding to 5 km/s) is given to each mesh point in the middle panel. The right panel shows noise map.

with one-channel and two-channel data are 0.357 and 0.239, respectively. Similarly, the value of MAEs for the model with one-channel and two-channel data are 0.265 and 0.188, respectively. In this case, it is again observed that two-channel data outperforms one-channel data as it has higher accuracy and lower RMSE and MAE values.

(3) We have combined the data from both disk and elliptical galaxies and thereby trained CNN with a large number of images (200,000). The overall accuracies for the combined dataset for one-channel and two-channel data are 94.6% and 95.9% respectively. Moreover, results for RMSEs for one-channel and two-channel data are 0.733 and 0.595, respectively. It is also observed that MAEs for combined dataset (disk+elliptical) for model with one-channel and two-channel data are 0.501 and 0.367, respectively. This shows that two-channel data again outperforms one-channel data for this. These results imply that the new method can be applied to different types of galaxies with GCSs.

(4) We have also used a CNN with two more convolutional layers in order to improve accuracy. We have found that our accuracy for the model with combined data (disk+ elliptical galaxies) is increased by 3% for one-channel (97.6%) and 2% for two-channel (97.8%). The RMSEs for the new architecture are 0.539 and 0.51 for one-channel and two-channel, respectively. Moreover, MAEs for the model with one-channel and two-channel data are 0.288 and 0.275, respectively. Hence, it is observed that the accuracies of the model (one-channel and two-channel) are significantly improved with the addition of two more convolutional layers in the existing architecture.

(5) In the above tests, we have used 80% of the original data for training CNNs and used the 20% for testing. This means that the testing dataset can be similar to the training data to some extent, because the two dataset generated from GCSs in the same simulated galaxies. In order to do a more stringent test for the new CNNs, we have applied our CNN to completely unknown data that is not at all even for training. We have confirmed that our CNN can accurately predict the galaxy masses for this completely unknown data.

(6) We have found that CNN trained by 200,000 images containing Gaussian noise predicts the total masses of with the accuracy of 80.9%, which implies that the prediction accuracy is still good, though it needs to be improved through the revision of the CNN architecture in our future studies.

(7) Although we have successfully demonstrated that the new method can accurately predict the total masses of galaxies, the simulated GCS kinematics can be very limited (not so diverse as real observations). Therefore, in order to apply the method to real observations, we need to dramatically increase the number of 2D kinematics maps of GCSs that cover a large range of the possible GCS kinematics in real galaxies. Thus we will use the predictions from cosmological simulations of galaxy formation with GCS models in order to train our CNNs in our future studies.

6 ACKNOWLEDGMENT

We are grateful to the referee for constructive and useful comments that improved this paper.

7 DATA AVAILABILITY

The data underlying this article will be shared on a justified request to the corresponding author.

REFERENCES

- Alabi A. B., et al., 2016, *Monthly Notices of the Royal Astronomical Society*, 460, 3838
- Alabi A. B., et al., 2017, *Monthly Notices of the Royal Astronomical Society*, 468, 3949
- Bahcall J. N., Tremaine S., 1981, *The Astrophysical Journal*, 244, 805
- Bekki K., 2013, *Monthly Notices of the Royal Astronomical Society*, 432, 2298–2323
- Bekki K., Couch W. J., Forbes D. A., Beasley M. A., 2005, *Highlights of Astronomy*, 13, 191
- Bekki K., Yahagi H., Nagashima M., Forbes D. A., 2008, *Monthly Notices of the Royal Astronomical Society*, 387, 1131
- Bekki K., Diaz J., Stanley N., 2019, *Astronomy and Computing*, 28, 100286
- Boylan-Kolchin M., 2018, *Monthly Notices of the Royal Astronomical Society*, 479, 332
- Brodie J. P., Strader J., 2006, *Annual Review of Astronomy and Astrophysics*, 44, 193
- Brodie J. P., et al., 2014, *The Astrophysical Journal*, 796, 52
- Cavanagh M., Bekki K., 2020, *arXiv e-prints*, p. arXiv:2006.14847
- Diaz J. D., Bekki K., Forbes D. A., Couch W. J., Drinkwater M. J., Deeley S., 2019, *Monthly Notices of the Royal Astronomical Society*, 486, 4845
- Dieleman S., Willett K. W., Dambre J., 2015, *Monthly Notices of the Royal Astronomical Society*, 450, 1441
- Dolfi A., et al., 2020, *Monthly Notices of the Royal Astronomical Society*, 495, 1321
- Forbes D. A., Read J. I., Gieles M., Collins M. L. M., 2018, *Monthly Notices of the Royal Astronomical Society*, 481, 5592
- Géron A., 2017, *Hands-on machine learning with Scikit-Learn and TensorFlow : concepts, tools, and techniques to build intelligent systems*. O'Reilly Media, Sebastopol, CA
- Griffen B. F., Drinkwater M. J., Iliev I. T., Thomas P. A., Mellema G., 2013, *Monthly Notices of the Royal Astronomical Society*, 431, 3087
- Hariharan B., Arbeláez P., Girshick R., Malik J., 2017, *IEEE Transactions on Pattern Analysis and Machine Intelligence*, 39, 627
- Hinton G. E., Srivastava N., Krizhevsky A., Sutskever I., Salakhutdinov R. R., 2012, *arXiv e-prints*, p. arXiv:1207.0580
- Krizhevsky A., Sutskever I., Hinton G. E., 2012, *Communications of the ACM*, 60, 84
- Krizhevsky A., Sutskever I., Hinton G. E., 2017, *Communications of the ACM*, 60, 84–90
- Morganti L., Gerhard O., Coccato L., Martinez-Valpuesta I., Arnaboldi M., 2013, *Monthly Notices of the Royal Astronomical Society*, 431, 3570
- Navarro J. F., Frenk C. S., White S. D. M., 1996, *The Astrophysical Journal*, 462, 563
- Neto A. F., et al., 2007, *Monthly Notices of the Royal Astronomical Society*, 381, 1450
- Peng E. W., Ford H. C., Freeman K. C., 2004, *The Astrophysical Journal*, 602, 705
- Pfeffer J., Kruijssen J. M. D., Crain R. A., Bastian N., 2017, *Monthly Notices of the Royal Astronomical Society*, 475, 4309
- Prole D. J., et al., 2019, *Monthly Notices of the Royal Astronomical Society*, 484, 4865
- Romanowsky A. J., Douglas N. G., Arnaboldi M., Kuijken K., Merrifield M. R., Napolitano N. R., Capaccioli M., Freeman K. C., 2003, *Science*, 301, 1696
- Santos M. G., Cooray A., Haiman Z., Knox L., Ma C.-P., 2003, *The Astrophysical Journal*
- Simonyan K., Zisserman A., 2014, *arXiv e-prints*, p. arXiv:1409.1556
- Spitler L. R., Romanowsky A. J., Diemand J., Strader J., Forbes D. A., Moore B., Brodie J. P., 2012, *Monthly Notices of the Royal Astronomical Society*, 423, 2177
- Su Y., Gu L., III R. E. W., Irwin J., 2014, *The Astrophysical Journal*, 786, 152
- Watkins L. L., Evans N. W., An J. H., 2010, *Monthly Notices of the Royal Astronomical Society*, 406, 264